The Journal of Chemical Physics ARTICLE scitation.org/journal/jcp

Charge transfer plasmons in the arrays of nanoparticles connected by conductive linkers

Cite as: J. Chem. Phys. 154, 084123 (2021); doi: 10.1063/5.0040128
Submitted: 10 December 2020 • Accepted: 4 February 2021 •
Published Online: 26 February 2021

View Online Export Citation CrossMark

A. S. Fedorov,[1,2,3,a] M. A. Visotin,[1,2] V. S. Gerasimov,[1,4] S. P. Polyutov,[1,5,b] and P. A. Avramov[6]

AFFILIATIONS

[1] International Research Center of Spectroscopy and Quantum Chemistry—IRC SQC, Siberian Federal University, Krasnoyarsk 660041, Russia
[2] Kirensky Institute of Physics, Federal Research Center KSC SB RAS, Krasnoyarsk 660036, Russia
[3] National Research Tomsk State University, Tomsk 634050, Russia
[4] Institute of Computational Modelling, Federal Research Center KSC SB RAS, Krasnoyarsk 660036, Russia
[5] Federal Siberian Research Clinical Centre under FMBA of Russia, Krasnoyarsk 660037, Russia
[6] Kyungpook National University, Daegu 41566, South Korea

[a] **Electronic mail:** alex99@iph.krasn.ru
[b] **Author to whom correspondence should be addressed:** spolyutov@sfu-kras.ru

ABSTRACT

Charge transfer plasmons (CTPs) that occur in different topology and dimensionality arrays of metallic nanoparticles (NPs) linked by narrow molecular bridges are studied. The occurrence of CTPs in such arrays is related to the ballistic motion of electrons in thin linkers with the conductivity that is purely imaginary, in contrast to the case of conventional CTPs, where metallic NPs are linked by thick bridges with the real optical conductivity caused by carrier scattering. An original hybrid model for describing the CTPs with such linkers has been further developed. For different NP arrays, either a general analytical expression or a numerical solution has been obtained for the CTP frequencies. It has been shown that the CTP frequencies lie in the IR spectral range and depend on both the linker conductivity and the system geometry. It is found that the electron currents of plasmon oscillations correspond to minor charge displacements of only few electrons. It has been established that the interaction of the CTPs with an external electromagnetic field strongly depends on the symmetry of the electron currents in the linkers, which, in turn, are fully governed by the symmetry of the investigated system. The extended model and the analytical expressions for the CTPs frequencies have been compared with the conventional finite difference time domain simulations. It is argued that applications of this novel type of plasmon may have wide ramifications in the area of chemical sensing.

Published under license by AIP Publishing. https://doi.org/10.1063/5.0040128

I. INTRODUCTION

Localized surface plasmons (LSPs) have attracted a great deal of attention by the ability to strengthen local electromagnetic fields in different optical processes, which can be important for many applications. An LSP represents oscillations of free electrons and electromagnetic fields induced by the charge motion inside conductive nanoparticles (NPs).[1,2] Plasmonic materials are currently used in photovoltaic cells,[1,3–6] water splitting,[7] chemical synthesis,[8] plasmon lasers,[9] biomedicine and telecommunication,[10,11] high-resolution imaging,[12] and so on. In addition, the LSP resonances find wide applications in chemical and biological sensing.[13–17] The properties of such sensors are often determined by the high sensitivity of the surface resonant frequency (SRF) to the permittivity of the chemical environment, which leads to the frequency shift caused, for example, by chemical adsorption.[14–16,18]

The SRF strongly depends on the shape and size of NPs and a material separating them.[1,2,14–18] This is due to the strong dependence of the LSP electromagnetic field on the interparticle spacings. This causes a vast variety of shapes of plasmonic structures, including individual NPs of different shapes and materials[19] and 2D lattices.[10,11,20,21]

Published under license by AIP Publishing

A significant contribution to understanding the electronic excitations in different systems, e.g., bulk 3D systems, molecular chains, and clusters, was made by Bernadotte *et al.*[22] It was shown that the concept of plasmons is applicable even to molecules. Using a step-by-step analysis, the authors systematized the electronic excitations in these systems and demonstrated two types of excitations defined by the poles of the external response function,

$$\chi_{ext}(r, r', \omega) = \int \varepsilon^{-1}(r, r'', \omega)\chi_{irr}(r'', r', \omega)d^3r''.$$

The type-I excitations form a quasi-continuum of the single-particle excitations that emerges from the poles of irreducible response function χ_{irr}. The type-II excitations are the plasmon excitations originating from zero eigenvalues of dielectric function ε at a certain frequency.

It was shown using the time-dependent density-functional theory (TDDFT)[23] that, for a periodic 1D system, the plasmon frequency ω_{pl} depends on the wave vector q and turns to zero at $q \to 0$. At the same time, for the model of a finite wire or molecular systems such as the Na_{20} chain or a tetrahedral cluster, the plasmon frequency was several times higher than the HOMO–LUMO gap.

The presence of a conductive material between two NPs leads to the occurrence of a new mode called charge transfer plasmon (CTP), in which the charge periodically moves between two NPs through a conductive bridge. The CTPs were experimentally observed in a system of two Au NPs linked by a thick gold bridge with a radius from 10 nm to 20 nm.[15] In Ref. 24, the CTPs were detected using the scattering spectra for bridged gold disk dimers with a nanowire diameter and length of 95 nm and 30 nm, respectively, and a nanowire width from 15 nm to 60 nm. For such systems, it was shown that the reduction in the conductivity of a bridge via decreasing its diameter results in the shift of the CTP resonance to the near- and mid-infrared spectral ranges.

The quantum properties of the CTPs supported by a metallic dimer bridged with a two-level system (TLS), representing an atom, a molecule, etc., were studied by the TDDFT approach in Ref. 25. It was shown that CTP appears when an energy level of the TLS is resonant with the Fermi level of both metallic nanoparticles. It enables electrons to flow through the junction. At the resonance, the TLS conductance becomes close to one quantum of conductance $G_0 = 2e^2/h$.

In Ref. 26, a first-principles study of the plasmonic response of a stretched metallic nanorod was performed. A quantized evolution of the plasmon modes during the nanorod stretching has been described, and a correlation between discontinuities of the plasmons and the discrete number of conduction channels in the break junction was established. It can be treated as the plasmonic analog of quantization conduction in atomic-scale junctions.

In Ref. 27, an optical response of two Na_{380} clusters during their approach and retract processes was calculated on the basis of TDDFT theory and in conjunction with the SIESTA package. It was demonstrated that due to the quantization of the conductance in metal nanocontacts, atomic-scale reconfigurations play a crucial role in determining the optical response of the whole system. The authors observed sudden changes in the intensities and spectral positions of plasmon frequencies and found a one-to-one correspondence between these changes and the quantized transport as the neck cross section diminishes.

In Ref. 28, the response of a plasmonic trimer metamolecule with the trigonal D3h symmetry was explored. The near-field response was measured with the nanoscale resolution using a molecular probe under the circularly polarized light excitation. The experiments showed that the near-field optical chirality can be imprinted into a photosensitive polymer and used in polarization-sensitive photochemistry.

The CTPs of this type can be described in terms of the classical Maxwell electrodynamics since the quantum effects were not expected to be significant there because of the relatively large NP and bridge sizes. However, later on, the quantum effects of the CTPs were investigated in the systems consisting of two NPs separated by subnanometer gaps.[29–31] In such systems, the coupling between NPs is determined by the interparticle tunneling and screening effects.

In addition, note that the NP structures with conducting 1,4-benzenedithiolate (BDT) and biphenyl-4,4-dithiol (BPDT) molecules linking cuboidal silver NPs[32] and gold monolayers,[33] respectively, were examined. It was shown that the presence of conductive linkers leads to the occurrence of a screened coupled plasmon mode and a shift of the coupled plasmon energy. When a biphenyl-l-4-thiol molecule was used instead of BPDT,[33] a chemical bond was formed through only one sulfur atom linked to one of the two Ag NPs (therefore, this cannot be a conductor); when an insulating 1,2-ethanedithiolate molecule was used instead of conductive BDT,[32] these effects were not observed.

Previously,[34,35] we studied a system of NP pairs linked by narrow conductive molecular bridges, expecting the pronounced quantum effects, and developed a hybrid model for describing CTPs in such systems. In this work, we further develop the hybrid model for the accurate description of more complex systems, taking into account some quantum effects, and derive a general analytical expression for the plasmonic frequencies of such NP systems.

II. MODEL OF THE CTP IN ARRAYS OF METALLIC NANOPARTICLES LINKED BY CONDUCTIVE MOLECULES

Here, we follow the basic ideas of the model outlined in our previous works[34,35] where the NP size is small, the interparticle bridge is only a narrow conductive molecular polymer chain, and carriers move in the ballistic mode. The ac current of the ballistically moving carriers accumulates the kinetic energy, which periodically flows into the potential energy of charged particles. It should be noted that, in the proposed model, there is no loss in the total energy of the system.

We also assume that, due to similarity, the local dynamics of the carriers in this narrow bridge and in the corresponding periodic (nanoparticle-bridge) system should be similar. In addition, we assume that the kinetic energy of every free carrier exhibits the parabolic dependence $E(k) = \frac{(\hbar k)^2}{2m^*}$ on the carrier wave vector k and is inversely proportional to the carrier effective mass m^*.

The total kinetic energy E_{kin} of free carriers in the bridge can be written as a sum of electrons in the conduction band with different

Published under license by AIP Publishing

quasi-momenta,

$$E_{kin} = \sum_{k,n} n_{k,n} \frac{\hbar^2 k_{k,n}^2}{2m^*}, \tag{1}$$

where $n_{k,n}$ are the occupancies for the electrons with the quasi-momentum k_k and the band number n. Under the action of a weak electric field, carriers are only excited near the Fermi level, so the kinetic energy derivative is

$$\frac{dE_{kin}}{dt} = n_f \frac{\hbar k}{m^*} \left[\frac{d(\hbar k)}{dt} \right]_{k=k_f}, \tag{2}$$

where n_f are the occupancies for the electrons with the Fermi quasi-momentum $k = k_f$. Due to the spin degeneracy and generation of holes with the same effective mass upon excitation of electrons near the Fermi level, below we limit the consideration to the electrons with $n_f = 4$.

The total time-dependent current $I(t)$ in a 1D bridge can be calculated as[36]

$$I(t) = \frac{-e}{L} \sum_{k,n} n_{k,n} v_{k,n}^{eff}, \tag{3}$$

$$v_{k,n}^{eff} = \frac{1}{\hbar} \frac{\partial E(k,n)}{\partial k} = \frac{\hbar k_{k,n}}{m^*}, \tag{4}$$

where L is the bridge length and $v_{k,n}^{eff}$ is the electron effective velocity.

The total current in a bridge is nonzero because the $n_{k,n}$ values for the quasi-momentum of electrons moving in the bridge in the opposite directions are different due to the difference between the electrochemical potentials of NPs.

Assuming that, at the weak oscillations, carriers are only excited near the Fermi level and taking into account Eq. (1), we can write the total kinetic energy E_{kin} of the free carriers forming the current $I(t)$ in the bridge as

$$E_{kin} = \frac{L^2 m^*}{2 n_f e^2} I(t)^2 = \frac{\alpha I(t)^2}{2}, \tag{5}$$

where the coefficient is

$$\alpha = \frac{L^2 m^*}{n_f e^2}. \tag{6}$$

In Ref. 34, we proved that the potential energy of all investigated charged (from $-2e$ to $+2e$) gold NPs with a number of atoms ranging from 55 to 1415 is well-approximated by the quadratic function of the charge

$$E_{pot} = aQ^2 + bQ + c \tag{7}$$

with the determination coefficient R^2 above 0.9999. In these quadratic functions, the coefficient c is the total energy and the coefficient b is the opposite value of the Fermi energy of a corresponding neutral NP. According to the classic electrostatics, the electrostatic energy of a charged sphere is $E = Q^2/(2C)$, so the coefficient a is related to the capacity C as $C = 1/(2a)$.

For all NPs studied in Ref. 34, it was found that their capacities are consistent with the NP radius R (in the atomic system of units), which was confirmed also by electrostatics of charged spheres.

Based on the aforesaid, we can draw an important conclusion that the additional charge of an NP is fully localized on its surface. All this allows us to use the formula for the potential energy of an isolated charged NP,

$$E_{pot} = \frac{Q^2}{2R} + bQ + c,$$

where Q is the NP charge.

Following the proposed model for dumbbell structures consisting of two NPs with radius R linked by a conductive bridge with length L, one can see that the NPs have the opposite electrostatic charges $Q_1(t)$ and $Q_2(t) = -Q_1(t)$ and the potentials φ_1 and φ_2 on the surface of both NPs are

$$\varphi_1 = \frac{Q_1}{R} + \frac{Q_2}{2R+L}, \ \varphi_2 = \frac{Q_2}{R} + \frac{Q_1}{2R+L}. \tag{8}$$

According to Eq. (3), the potential difference results from the charge transfer during the plasmon oscillations with the current $I(t) = \frac{dQ(t)}{dt}$ in the bridge.

Formally, the dumbbell structure we study can be considered to be an LC oscillatory circuit, in which the total potential energy of two NPs is

$$E_{pot} = \frac{Q^2}{R} - \frac{Q^2}{2R+L}.$$

In Refs. 37 and 38, it was proposed to correct this formula in order to take into account the self-consistent dipole polarization of spheres during their interaction as

$$E_{pot} = \frac{Q^2}{R} - \frac{F(R,L)Q^2}{2R+L},$$

where the correction function $F(R, L)$ is the difference between the interactions of two conductive spheres (NPs) and point charges at the center of a polarized sphere. In Ref. 38, it was shown that this function rapidly decreases from 2.0, when two conducted spheres are in contact, to 1.0, when $\frac{L}{2R} \to \infty$ and $[F(R, L)] \simeq 1.07$ at $\frac{L}{2R} = 1.4$. Taking into account that this function rapidly drops to 1.0 and recalling that here we study the systems with $L \geq (2R)$, below we omit $F(R, L)$ in all the equations.

Thus, the sum of the NP–bridge–NP system potential and the kinetic energies is similar to the total energy of the LC circuit,

$$E_{tot} = E_{pot} + E_{kin} = \left(\frac{Q(t)^2}{R} - \frac{Q(t)^2}{2R+L} \right) + \frac{\alpha I(t)^2}{2}. \tag{9}$$

Assuming the absence of the total energy dissipation, by differentiation of Eq. (9) and dividing the result by $I(t)$, we arrive at the differential equation of the harmonic oscillations, which contains the squared modified plasmonic frequency $\widetilde{\omega_{pl}^2}$,

$$\frac{d^2Q(t)}{dt^2} = -\widetilde{\omega_{pl}^2} Q(t), \ \widetilde{\omega_{pl}^2} = \left(\frac{1}{R} - \frac{1}{2R+L} \right) \frac{2}{\alpha} = 2\beta, \tag{10}$$

Published under license by AIP Publishing

where the introduced parameter β is the squared frequency,

$$\beta \equiv \frac{1}{\alpha}\left(\frac{1}{R} - \frac{1}{2R+L}\right). \tag{11}$$

Thus, the dynamics of the NP–bridge–NP system and the LC circuit is the same, even though the nature of the energy related to the current $I(t)$ is completely different. In the LC circuit, the energy is the current in a magnetic field, while in the NP–bridge–NP system, the energy is the kinetic energy of free carriers in the bridge. This ballistic current in the bridge is changed for the acceleration of carriers in an electric field of charged NPs.

III. VERIFICATION OF THE CTP MODEL BY THE FDTD SIMULATION

In order to test the feasibility of the proposed model, we below compare the plasmon frequency calculated using both the proposed model and exact Finite-Difference Time-Domain (FDTD) calculations for the simple systems. Specifically, plasmon frequencies were calculated for a dimer and for an equilateral triangle of identical nanoparticles connected by conducting linkers. It should be noted that calculations of plasmon frequencies for complex systems by the FDTD method, especially for 3D systems of many connected nanoparticles, are very time consuming. At the same time, the calculations of the plasmon frequencies of complex systems using the developed model are extremely simple and fast.

A. Permittivity of a material with the ballistic carrier transport for the FDTD calculation

Under the assumption that free carriers (electrons and holes) move in 1D conductive linkers in the ballistic mode, we can consider these carriers to be particles with effective mass m^* under the action of only a local electric field. If n is the carrier density in the linker, then their motion at velocity v creates the current density,

$$j = env. \tag{12}$$

In the Finite-Difference Time-Domain (FDTD) simulation, conductive linkers can be modeled by thin cylinders with length L and radius r. If the periodic external field $E(t) = E_0 \exp(-i\omega t)$ with frequency ω is applied along the cylinder axis, one should expect that electrons will also move back and forth along the cylinder axis at the same frequency.

Here, we assume that the photon energy $\hbar\omega$ is lower than the gap between the occupied and unoccupied nonconductive energy levels, so the polarizability of a linker in molecular orbitals can be ignored and only conductive carriers respond to an external electric field. This means that the polarization of the linker medium is caused by the intraband excitations, as in the Drude model, but without scattering. In addition, we ignore the polarizability of a conductive linker in the direction perpendicular to its axis, thereby setting the permittivity in this direction to be ε_0.

The acceleration of an electron along the linker can be written as

$$\frac{dv}{dt} = \frac{e}{m^*} E_0 \exp(-i\omega t). \tag{13}$$

Integrating Eq. (13) over time and substituting the result into Eq. (12), we find the current density

$$j(t) = en \cdot \frac{e}{m^*} \frac{E_0 \exp(-i\omega t)}{-i\omega} = i\frac{e^2 n}{\omega m^*} E(t). \tag{14}$$

Since the optical conductivity is, by definition, the ratio between the current density and the electric field, we can write the frequency-dependent complex optical conductivity and the complex permittivity (in the SI units) of the conductive linker in the form

$$\sigma(\omega) = i\frac{e^2 n}{\omega m^*}, \tag{15}$$

$$\varepsilon(\omega) = \varepsilon_0 - \frac{e^2 n}{\omega^2 m^*}, \tag{16}$$

where ε_0 is the permittivity of vacuum.

The ballistic transport mode makes the conductivity purely imaginary and the permittivity purely real, which excludes attenuation in the medium. This is obviously due to the fact that carriers do not experience scattering, and therefore, there is no energy dissipation in the linker. In contrast to this, conventional metals with a short electron mean free path conduct in the drift-diffusion mode and are characterized by the real optical conductivity.

B. FDTD calculation setup and post-processing

To verify the CTP frequencies obtained using our hybrid model, we employed the FDTD method implemented in the commercial package.[39] A standard simulation scheme was used. The structure was illuminated by a plane wave. The perfectly matched layer (PML) boundary conditions were established on all sides of a simulation cell, and the total-field scattered-field (TFSF) technique was used to reproduce the infinite space. The absorption cross section was calculated with a set of discrete Fourier transform (DFT) monitors surrounding a particle inside the TFSF region and the scattering cross section, with the monitors surrounding the entire TFSF region, so that they only read the scattered field. To accurately reproduce the particle shape, an adaptive mesh was used. In the current density calculation, the material was considered to be a homogeneous electron plasma cloud.

It is well-known[40] that, ignoring the magnetic susceptibility of a material, one can present the current as

$$\mathbf{J} = \frac{\partial \mathbf{P}}{\partial t}, \tag{17}$$

but, since $\mathbf{J} \propto e^{-i\omega t}$, we have

$$\mathbf{J} = -i\omega \mathbf{P}. \tag{18}$$

According to Ref. 40, the polarization vector and the electric field vector are related as

$$\mathbf{P} = \frac{\varepsilon - 1}{4\pi}\mathbf{E}. \tag{19}$$

Substituting this into Eq. (18), we obtain

$$\mathbf{J} = -i\omega\frac{\varepsilon - 1}{4\pi}\mathbf{E}. \tag{20}$$

Published under license by AIP Publishing

In all the FDTD simulations, we modeled the conductive linkers by cylinders with a length of $L = 2$ nm and a radius of $r = 0.2$ nm with the permittivities given by Eq. (16). The parameters of carriers were taken to be $m^* = 0.5\, m_e$ and $n = 1/\Omega = 1/(L\pi r^2)$. Gold NPs were modeled by spheres with a radius of $R = 1$ nm and the tabulated Au permittivity from Ref. 41.

Following Sec. II, below we generalize the approach developed in our previous work[34] and use it for more complex systems consisting of an arbitrary number of NPs with momentary charges Q_j connected by conductive linkers with currents I_{jk}.

Under the assumptions made in Ref. 34, we can divide the total energy of the system into two contributions: the electrostatic potential energy of NPs and the kinetic energy of charge carriers in the linkers,

$$E_{kin} = \sum_{jk} \frac{\alpha_{jk}}{2} I_{jk}^2, \tag{21}$$

$$E_{pot} = \sum_{j \neq k} \frac{Q_j Q_k}{R_{jk}} + \sum_j \{a_j Q_j^2 + b_j Q_j + c_j\}, \tag{22}$$

where α_{jk} corresponds to the conducting properties of a linker between the j-th and k-th particles [Eq. (5)], r_{jk} is the distance between the NP centers, and a_j, b_j, and c_j are the coefficients representing energy–charge dependence (7) for the j-th particle. In addition, we hereinafter imply the current I_{jk} is zero if $j = k$ or when the j-th and k-th particles are not linked.

The current I_{jk} transfers the charge from the j-th to k-th particle and that results in change of the potential energy. Since we expect the total energy of the system to be conserved, the decrease in the potential energy equals to the increase in the kinetic part, which is observed as an increase in the I_{jk} value,

$$(\varphi_j - \varphi_k) I_{jk} = \left(\frac{\partial E_{pot}}{\partial Q_j} - \frac{\partial E_{pot}}{\partial Q_k} \right) I_{jk} = \frac{\partial E_{kin}}{\partial I_{jk}} \frac{dI_{jk}}{dt}. \tag{23}$$

These energy balance equations should be supplemented with the continuity relations showing that the charge of a particle Q_j can only be changed by the current through the linkers connected to this particle,

$$\dot{Q}_j = -\sum_k I_{jk}. \tag{24}$$

Equations (23) and (24) form a well-defined system, which is sufficient to solve the charge dynamics in the NP.

For simplicity, hereafter, we treat all the particles and linkers as identical and set a_j [the quadratic term in Eq. (7)] to be inversely proportional to $2R$, where R is the NP radius. All the linear terms b_j in Eq. (23) cancel out. Substituting the partial derivatives in (23) and dividing both sides by I_{jk}, we arrive at

$$\sum_{s \neq j,k} Q_s \left(\frac{1}{R_{sj}} - \frac{1}{R_{sk}} \right) + (Q_j - Q_k) \left(\frac{1}{R} - \frac{1}{R_{jk}} \right) = \alpha \dot{I}_{jk}. \tag{25}$$

Taking the time derivative of Eq. (24) and substituting Eq. (25) into it, we can obtain a system of second-order differential equations for the particle charges

$$\ddot{Q}_j = -\frac{1}{\alpha} \sum_k{}' \left(\sum_{s \neq j,k} Q_s \left(\frac{1}{R_{sj}} - \frac{1}{R_{sk}} \right) + (Q_j - Q_k) \left(\frac{1}{R} - \frac{1}{R_{jk}} \right) \right), \tag{26}$$

where the first (primed) summation is made only over the particles connected to the j-th particle by a linker.

To obtain the equivalent equations for the time evolution of the currents inside the linkers, one should put (24) to the time derivative of (25), which yields the second-order differential equation

$$\sum_{s \neq j,k} \left(\sum_t I_{st} \left(\frac{1}{R_{sj}} - \frac{1}{R_{sk}} \right) \right) + \sum_t (I_{jt} - I_{kt}) \left(\frac{1}{R} - \frac{1}{R_{jk}} \right) = -\alpha \ddot{I}_{jk}. \tag{27}$$

In this work, we use the latter formulation to find the current oscillation frequencies.

IV. CTP CALCULATIONS FOR DIFFERENT NP ARRAYS

Here, we study the frequencies ω^ν and the corresponding eigenvectors of the currents I_{ij}^ν in linkers for the CTPs in different complexes (Fig. 1) consisting of identical NPs with radius R connected by identical conductive linkers with length L and parameter α [see Eq. (5)].

It is interesting to perform a symmetry analysis of the plasmonic oscillations described by the currents between nanoparticles for all the complexes studied (see Fig. 1).

It should be taken into account that, despite the symmetry of the geometric arrangement of the particles, due to the vector nature of the currents shown in Fig. 1 by arrows, the point symmetry for all systems is lower than the symmetry of the particles in them. The only exception is the four-rayed star that has D_4 symmetry.

The lowest symmetry is in a linear chain and in a tetrahedron that both have only one symmetry element E due to the asymmetric directions of currents.

In other cases, the systems have cyclic Abelian symmetry groups. The triangle has C_3 symmetry possessing elements E, C_3, C_3^2. Similarly, the square has C_4 symmetry and the hexagon has C_6 symmetry. All of these groups possessing only one-dimensional irreducible representations. Each symmetry element C_n^m has a representation character equal to $e^{\frac{2\pi i}{n} m}$. One of these representations is a completely symmetric representation, having character $e^{\frac{2\pi i}{n} 0} = 1$ corresponding to a constant current through each linker. Due to the homogeneity of the currents, the plasmon frequency for this symmetric representation is zero for all of these three systems.

Because of cyclic characters $e^{\frac{2\pi i}{n} m}$, there are representations for the square and the hexagon that lead to symmetric and antisymmetric plasmonic oscillations in these systems (see text below and Fig. 5).

The D_4 symmetry of four-rayed star has five irreducible representations: four of them are one-dimensional and one is two-dimensional. One irreducible representation is completely symmetric (breathing mode). However, unlike the other systems with Abelian groups, this representation leads to the maximum change of potential energy at a homogeneous charge displacement and, therefore, has a maximum plasmon frequency (see text below).

Published under license by AIP Publishing

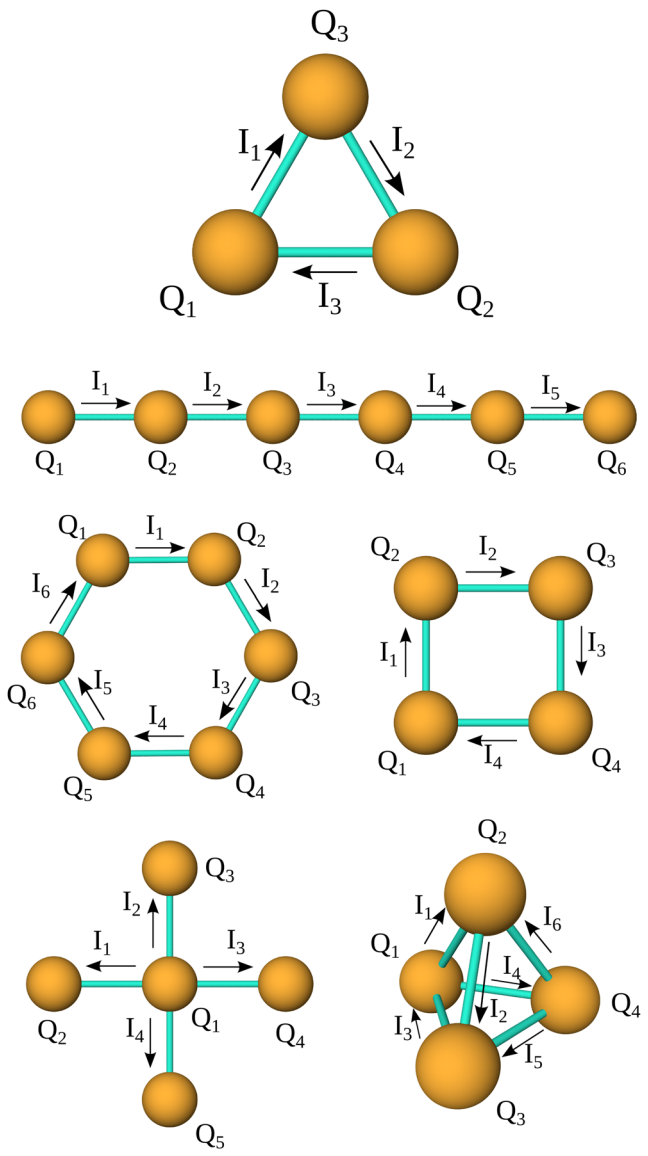

FIG. 1. Investigated CTP complexes.

A. CTPs in regular triangle

Following Eq. (27), we can easily obtain the equations

$$\alpha \dot{I}_1 = (\varphi_1 - \varphi_2), \tag{28}$$

$$\varphi_1 = \left(\frac{Q_2 + Q_3}{\tilde{L}}\right) + \frac{Q_1}{R}, \tag{29}$$

$$\varphi_2 = \left(\frac{Q_1 + Q_3}{\tilde{L}}\right) + \frac{Q_2}{R}, \tag{30}$$

$$\dot{Q}_1 = I_3 - I_1. \tag{31}$$

Here, we introduce the quantity $\tilde{L} = 2R + L$. This intercenter distance is convenient to use in calculating the interaction of charged NPs.

By the time differentiation of Eqs. (29)–(31) and using Eq. (31), we obtain

$$\alpha \ddot{I}_1 = \left(\frac{1}{R} - \frac{1}{\tilde{L}}\right)(I_2 + I_3 - 2I_1). \tag{32}$$

Rearranging cyclically the indices and assuming the harmonic time dependence of each current $I(t) \sim e^{i\omega t}$, we obtain the secular equation, where β was defined in (11),

$$\begin{bmatrix} 2\beta - \omega^2 & -\beta & -\beta \\ -\beta & 2\beta - \omega^2 & -\beta \\ -\beta & -\beta & 2\beta - \omega^2 \end{bmatrix} \begin{bmatrix} I_1 \\ I_2 \\ I_3 \end{bmatrix} = 0. \tag{33}$$

Solving this equation analytically, we get a solution with the squared frequency $\omega^2 = 0$ and the eigenvector $I = [0, 0, 0]$ corresponding to the dc current. Another $\omega^2 = 3\beta$ is doubly degenerate and corresponds to the eigenvectors $I = [-1, 1, 0]$ and, further, by the cyclic permutation of the indices corresponding to the current from one NP to two others with the same value (Fig. 1). It is interesting to compare the squared frequency of this system with that of the dimer system $\omega^2 = 2\beta$, Eq. (10).

B. Comparison of the analytical CTP frequencies with the FDTD data

Figure 2 shows the extinction spectra for the dimer and trimer of gold NPs.

One can see that the CTP for the dimer arises at $\lambda = 4.48$ μm. For this dimer, the calculation of the CTP frequency and wavelength using Eq. (10) yields a wavelength of $\lambda = 4.51$ μm, which shows excellent agreement between the results obtained using the proposed model for calculating the CTPs and the FDTD simulation. In addition, we used the FDTD simulation to investigate the CTPs in a regular triangle with the same NPs and linkers as in the dimer. According to the extinction peak position, the wavelength for this triangle CTP is 3.860 μm in the asymmetric case, when the external field is polarized along one of the triangle sides and 4.01 μm in the symmetric case (see also Fig. 2). The difference between the CTP positions obtained by the FDTD method can be attributed to the dipole–dipole interaction, which is ignored in the proposed model.

According to the proposed model [see (10)] and Subsection IV A, the triangle plasmon frequency should be $\sqrt{\frac{3}{2}}$

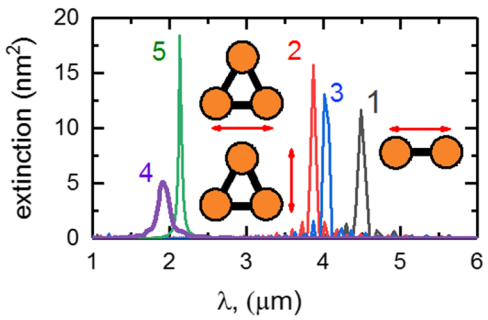

FIG. 2. Absorption spectra of (1) dimer (black) and trimer structures for (2) the vertical (red) and (3) horizontal (blue) polarizations of the external field. [(4) and (5)] Spectra for the Au dimer with the Au linker and with the linker with $\Re(n_{Au}) = 0$.

Published under license by AIP Publishing

times higher than that for the dimer. This gives the triangle CTP wavelength $\lambda \simeq 3.682\,\mu$m, which is only 4.8% different from the result of FDTD simulations. We again explain the difference in CTP frequencies obtained by FDTD method and the proposed model by the dipole–dipole interaction, which is neglected in the model.

Figure 2(4) shows the extinction spectra for the Au dimer with a linker characterized by the frequency-dependent permittivity of gold, and Fig. 2(5) presents the spectrum for the same dimer, but with a linker material with the zero real part of the refractive index. One can see that replacing the purely real permeability of the linker [Eq. (16)], leading to ballistic transport, by the permeability of gold or by the permeability leading to the imaginary refractive index, we obtain a significant decrease in the plasmon wavelength as compared with the case of a ballistic linker.

It should be noted that, in all the cases, the system exhibits a resonant peak in the visible wavelength range, which corresponds to an individual plasmon of a gold NP, and the frequency of this peak remains almost unchanged at any linker permittivity.

Figure 3 shows the current configuration at the CTP wavelength in the trimer structure calculated using Eq. (20) for both orientations of the external field. It is interesting to find the ratio between the CTP frequencies in this triangle and the dimer frequency. These ratios were found to be 1.16 and 1.12. According to the proposed model, this ratio should be $\sqrt{\frac{3}{2}} \simeq 1.22$ [see Eq. (10) and Subsection IV A]. We assume that the difference (up to 9.4%) between the ratios of the frequencies obtained using the FDTD calculation and the hybrid model is caused again by ignoring the dipole interactions in the model.

C. CTPs in a tetrahedron

For a tetrahedron (Fig. 1), a similar calculation yields the secular determinant

$$\begin{bmatrix} 2\beta-\omega^2 & -\beta & -\beta & \beta & 0 & \beta \\ -\beta & 2\beta-\omega^2 & -\beta & 0 & \beta & -\beta \\ -\beta & -\beta & 2\beta-\omega^2 & -\beta & -\beta & 0 \\ \beta & 0 & -\beta & 2\beta-\omega^2 & -\beta & -\beta \\ 0 & \beta & -\beta & -\beta & 2\beta-\omega^2 & \beta \\ \beta & -\beta & 0 & -\beta & \beta & 2\beta-\omega^2 \end{bmatrix}.$$

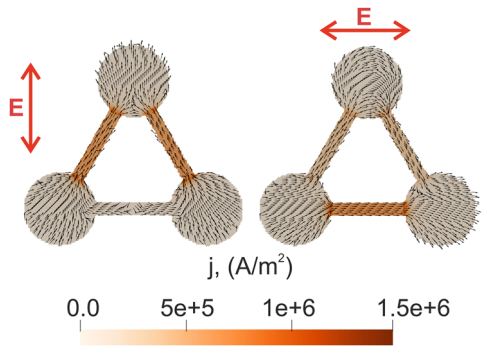

FIG. 3. Current density distribution for (a) the symmetric and (b) antisymmetric CTP configurations at the maximum extinction wavelengths calculated using the FDTD method.

The three solutions with a squared frequency of $\omega^2 = 0$ corresponded to the dc current flowing along the edges of one face, giving, for example, an eigenvector $I = [1, 1, 1, 0, 0, 0]$. Other triply degenerate solutions $\omega^2 = 4\beta$ correspond to the eigenvectors $I = [1, 0, -1, 1, 0, 0]$ and, similar, correspond to the currents from one NP toward the opposite face; all the three currents coincide.

D. CTPs in a square

For a square (Fig. 1), a similar calculation yields the secular determinant

$$\begin{bmatrix} 2*\beta-\omega^2 & \gamma-\beta & -2\gamma & \gamma-\beta \\ \gamma-\beta & 2\beta-\omega^2 & \gamma-\beta & -2\gamma \\ -2\gamma & \gamma-\beta & 2\beta-\omega^2 & \gamma-\beta \\ \gamma-\beta & -2\gamma & \gamma-\beta & 2\beta-\omega^2 \end{bmatrix},$$

where $\gamma \equiv \frac{1}{\alpha}\left(\frac{1}{L} - \frac{1}{\sqrt{2}L}\right)$.

Again, one solution has a squared frequency of $\omega^2 = 0$ corresponding to the dc current throughout all the vertices. The doubly degenerate frequency $\omega^2 = 2\beta + 2\gamma$ corresponds to the eigenvectors $I_2 = [-1, 0, 1, 0]$ and $I_3 = [0, -1, 0, 1]$ corresponding to the parallel currents from one square side to another. Another $\omega^2 = 4\beta - 4\gamma$ corresponds to the eigenvector $I = [-1, 1, -1, 1]$ and, similarly, corresponds to the equal currents from two opposite vertices to the other two.

E. CTPs in a four-rayed star

For a four-rayed star (Fig. 1), due to the higher complexity, we only present the frequencies and eigenvectors for the case $\tilde{L} \equiv 2R + L = 4R$. The matrix of all the eigenvectors is

$$\begin{bmatrix} -1 & 0 & -1 & 1 \\ 0 & -1 & 1 & 1 \\ 1 & 0 & -1 & 1 \\ 0 & 1 & 1 & 1 \end{bmatrix}.$$

The corresponding vector of the frequencies is $\omega^2 \simeq \frac{1}{R\alpha}[1.37, 1.37, 1.27, 5.98]$. The highest frequency corresponds to the fully symmetric eigenvector (the breathing mode). The doubly degenerate oscillations correspond to the two opposite currents from the opposite vertices. The lowest CTP oscillation corresponds to the flow of symmetric charges from the opposite vertices to another pair of vertices.

Curiously, for a given $\tilde{L}$ value, the oscillation frequency in a triangle is significantly lower than the breathing mode frequency $\omega^2 = \frac{2.25}{R\alpha}$, and for a dimer, the frequency is $\omega^2 = \frac{1.5}{R\alpha}$.

F. CTPs in 1D chains and coiled-up chains of nanoparticles

It is interesting to investigate the CTPs in the systems in the form of 1D chains of NPs connected by conductive linkers and follow the modification of plasmons in the system in the form of a coiled-up chain. For the basic configuration, we chose a chain of six NPs (Fig. 1) with $\tilde{L} \equiv 2R + L = 4R$ again. The oscillation frequency is

$$\omega^2 \simeq \frac{1}{R\alpha}[0.30, 0.94, 1.61, 2.15, 2.50].$$

Published under license by AIP Publishing

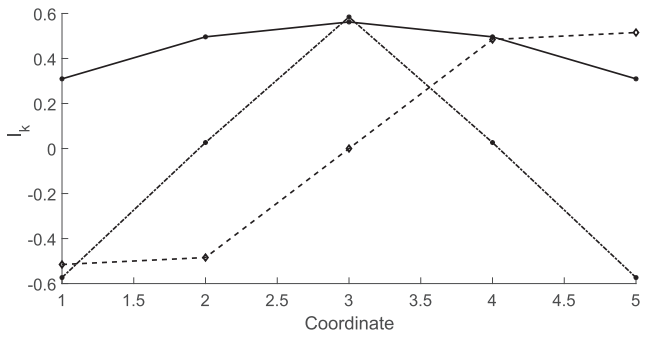

FIG. 4. Current along a chain of six particles. The solid line corresponds to the first CTP oscillation, the dashed line corresponds to the second one, and the dashed-dotted line corresponds to the third one.

Let us compare these values with the CTP frequency in a dimer with the same length: $\omega^2 = \frac{0.38}{R\alpha}$. It can be seen that the lowest frequency in the chain almost coincides with the plasmon in the dimer.

In addition, it is interesting to plot the dependence of all the eigenvectors, i.e., the currents in linkers, for all plasmons in the system (Fig. 4).

It can be seen that the vibrational modes are divided into symmetric and antisymmetric with respect to the center. In this case, indeed, the first vibrational mode in a system is similar to the vibration in the dimer consisting of two NPs and a linker.

Let us follow the evolution of the vibrational modes in this system when coiling the chain up. The oscillation frequency in the coil of six nanoparticles is

$$\omega^2 \simeq \frac{1}{R\alpha}[0.00, 0.98, 0.98, 2.19, 2.19, 2.65].$$

Here, we plotted four eigenvectors of the currents corresponding to the first, second, fourth, and sixth CTP oscillations (Fig. 5).

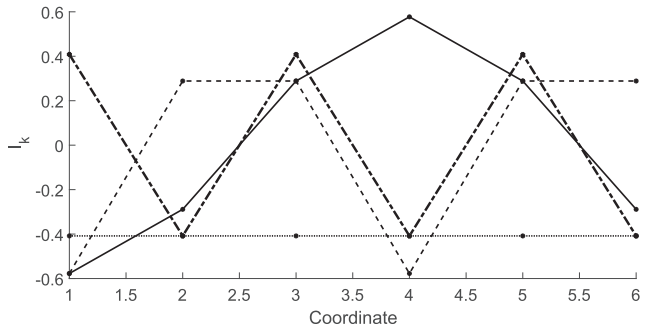

FIG. 5. Current in a coil of six particles. The dotted line corresponds to the first CTP oscillation, the solid line corresponds to the second one, the dashed line corresponds to the fourth one, and the dashed-dotted line corresponds to the last one.

To sum up, we plotted the dependences of the plasmon wavelengths for different typical investigated systems (dimer, triangle, and tetrahedron) on the radius of NPs forming the systems. In this case, the linker length was constant and equal to $L = 2$ nm and the linker conductivity was calculated using Eq. (6) at $n_f = 4$. These dependencies are presented in Fig. 6.

Using these dependencies, relating the plasmon quantum energy $\hbar\omega$ to the electrostatic energy $E_{pot} \simeq \frac{Q^2}{2R}$ of all NP charges in a system and to the kinetic energy of all the currents equal, on average, to these energies, we can estimate the characteristic charge of each NP in a system ($1e$–$3e$). Consequently, at these plasmon oscillations in the IR spectral range, a very small charge is transferred through the conducting bridges and the quantum blockade effect in the bridges is negligible.

G. Interaction of the CTPs with an external electromagnetic field

Knowing the relation between the time derivative of the charge of each NP and the currents passing through it [Eq. (24)], we can find the derivative of the dipole moment $\vec{P}$ for each vibrational mode using the formula

$$\dot{\vec{P}} = \sum_j \dot{Q}_j \vec{R}_j. \tag{34}$$

Assuming that the interaction of an external electromagnetic field with the plasmon oscillations is determined by the dipole moment of a system during this oscillation and, therefore, its time derivative [Eq. (34)], we can determine the optical activity of all the plasmonic modes in a system.

Calculating the CTP eigenvectors in the systems under study, we found that, due to the different symmetries of the CTP oscillations, all the oscillation modes are divided into optically active and inactive. For example, for a 1D chain (Fig. 1), the derivatives of the dipole moments for the three modes shown in Fig. 4 are $\dot{\vec{P}} \simeq [17.39, 0.00, -4.07]$.

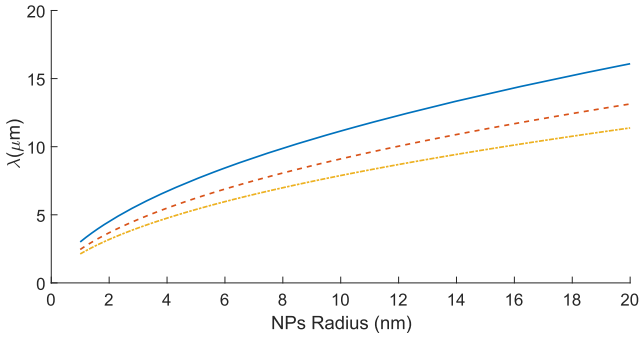

FIG. 6. Dependence of the CTP wavelength on the nanoparticle radius. The blue solid line corresponds to the CTPs in a dimer, the red dashed line corresponds to the CTPs in a triangle, and the yellow dashed-dotted line corresponds to the CTPs in a tetrahedron.

Published under license by AIP Publishing

Similarly, the derivatives of the dipole moments for the four modes in the six member ring shown in Fig. 5 are $\dot{P}_x \simeq [0.00, 6.93, 0.00, 0.00]$ and $\dot{P}_y \simeq [0.00, -12.00, -0.00, -0.00]$

V. CONCLUSIONS

Using the hybrid model, we investigated charge transfer plasmons in the arrays of metallic nanoparticles linked by narrow conductive molecular bridges. The model parameters can be obtained using *ab initio* simulations.

More precisely, the arrays in the form of a dimer, a regular triangle, a tetrahedron, a square, a four-rayed star, a linear chain, and a coiled-up linear chain were examined. The proposed model of charge transfer plasmons was based on the consideration of the energy flow between the electrostatic potential energy of charged nanoparticles and the kinetic energy of free carriers moving in a ballistic mode inside conductive linkers.

An important feature of this model is the ballistic motion of free carriers inside narrow linkers. The limited conductivity of the linkers together with sufficiently large distances between nanoparticles leads to a weak restoring force acting on free carriers in a system and, consequently, to the low plasmon oscillation frequency. It was shown that, for all the investigated systems, the plasmon frequencies lie in the IR spectral range.

The validity of the model used at the CTP frequencies in the dimer and trimer arrays was checked by the FDTD method. In this method, based on the numerical solution of Maxwell's equations for the electromagnetic field, the response of a system, which determines the plasmon oscillations, was calculated. In the calculation, we considered spherical metallic nanoparticles linked by narrow cylinders with the conductivity corresponding to that of conductive molecular bridges.

The ballistic transport mode causes the purely imaginary conductivity and the purely real permittivity, which means the absence of attenuation in the medium. In contrast to this, in the calculation of charge transfer plasmons in the systems of nanoparticles linked by thick bridges made of conventional metals, which have a short carrier mean free path, the bridges conduct in the drift-diffusion mode and exhibit the real optical conductivity.

The FDTD calculation revealed the excitations of two types. One of them lies in the visible wavelength range and corresponds to plasmons of individual particles, while the other lies in the infrared range and corresponds to the charge transfer plasmons. The FDTD calculation showed that the frequencies of these plasmons are in good agreement with the frequency determined using the proposed hybrid model.

We derived the general analytical or numerical equations for the CTP frequencies in the investigated systems. It was found that the currents flowing during these plasmon oscillations have a certain symmetry determined by the system geometry and the plasmons interact with an external electromagnetic field depending on the symmetry. It was established that the plasmon oscillation quanta correspond to minor displacements of a charge of few electrons.

Let us note that the chemical interaction of linkers with external molecules results in a strong change in the linker conductance that, in turn, directly leads to modification of the plasmon frequency that can be easily measured. It apparently provides the possibilities for utilization of CTPs with narrow conductive linkers for prospective chemical sensing.

ACKNOWLEDGMENTS

This study was supported by the Russian Science Foundation, Project No. 18-13-00363.

DATA AVAILABILITY

The data that support the findings of this study are available from the corresponding author upon reasonable request.

REFERENCES

[1] A. Uddin and X. Yang, "Surface plasmonic effects on organic solar cells," J. Nanosci. Nanotechnol. **14**, 1099–1119 (2014).
[2] J. Liu, H. He, D. Xiao, S. Yin, W. Ji, S. Jiang, D. Luo, B. Wang, and Y. Liu, "Recent advances of plasmonic nanoparticles and their applications," Materials **11**, 1833 (2018).
[3] F. Parveen, B. Sannakki, M. V. Mandke, and H. M. Pathan, "Copper nanoparticles: Synthesis methods and its light harvesting performance," Sol. Energy Mater. Sol. Cells **144**, 371–382 (2016).
[4] S. Gwo, H.-Y. Chen, M.-H. Lin, L. Sun, and X. Li, "Nanomanipulation and controlled self-assembly of metal nanoparticles and nanocrystals for plasmonics," Chem. Soc. Rev. **45**, 5672–5716 (2016).
[5] K. Ueno, T. Oshikiri, Q. Sun, X. Shi, and H. Misawa, "Solid-state plasmonic solar cells," Chem. Rev. **118**, 2955–2993 (2018).
[6] N. Venugopal, V. S. Gerasimov, A. E. Ershov, S. V. Karpov, and S. P. Polyutov, "Titanium nitride as light trapping plasmonic material in silicon solar cell," Opt. Mater. **72**, 397–402 (2017).
[7] M. Valenti, M. P. Jonsson, G. Biskos, A. Schmidt-Ott, and W. A. Smith, "Plasmonic nanoparticle-semiconductor composites for efficient solar water splitting," J. Mater. Chem. A **4**, 17891–17912 (2016).
[8] S. Linic, U. Aslam, C. Boerigter, and M. Morabito, "Photochemical transformations on plasmonic metal nanoparticles," Nat. Mater. **14**, 567–576 (2015).
[9] C. Deeb and J.-L. Pelouard, "Plasmon lasers: Coherent nanoscopic light sources," Phys. Chem. Chem. Phys. **19**, 29731–29741 (2017).
[10] V. S. Gerasimov, A. E. Ershov, R. G. Bikbaev, I. L. Rasskazov, I. V. Timofeev, S. P. Polyutov, and S. V. Karpov, "Engineering mode hybridization in regular arrays of plasmonic nanoparticles embedded in 1D photonic crystal," J. Quant. Spectrosc. Radiat. Transfer **224**, 303–308 (2019).
[11] V. I. Zakomirnyi, I. L. Rasskazov, V. S. Gerasimov, A. E. Ershov, S. P. Polyutov, and S. V. Karpov, "Refractory titanium nitride two-dimensional structures with extremely narrow surface lattice resonances at telecommunication wavelengths," Appl. Phys. Lett. **111**, 123107 (2017).
[12] K. A. Willets, A. J. Wilson, V. Sundaresan, and P. B. Joshi, "Super-resolution imaging and plasmonics," Chem. Rev. **117**, 7538–7582 (2017).
[13] D. N. Maksimov, V. S. Gerasimov, S. Romano, and S. P. Polyutov, "Refractive index sensing with optical bound states in the continuum," Opt. Express **28**, 38907 (2020).
[14] L. Guo, J. A. Jackman, H.-H. Yang, P. Chen, N.-J. Cho, and D.-H. Kim, "Strategies for enhancing the sensitivity of plasmonic nanosensors," Nano Today **10**, 213–239 (2015).
[15] A. N. Koya and J. Lin, "Charge transfer plasmons: Recent theoretical and experimental developments," Appl. Phys. Rev. **4**, 021104 (2017).
[16] N. Elahi, M. Kamali, and M. H. Baghersad, "Recent biomedical applications of gold nanoparticles: A review," Talanta **184**, 537–556 (2018).
[17] Z. Farka, T. Jurík, D. Kovář, L. Trnková, and P. Skládal, "Nanoparticle-based immunochemical biosensors and assays: Recent advances and challenges," Chem. Rev. **117**, 9973–10042 (2017).
[18] J. Olson, S. Dominguez-Medina, A. Hoggard, L.-Y. Wang, W.-S. Chang, and S. Link, "Optical characterization of single plasmonic nanoparticles," Chem. Soc. Rev. **44**, 40–57 (2015).

Published under license by AIP Publishing

[19]V. I. Zakomirnyi, I. L. Rasskazov, S. V. Karpov, and S. P. Polyutov, "New ideally absorbing Au plasmonic nanostructures for biomedical applications," J. Quant. Spectrosc. Radiat. Transfer **187**, 54–61 (2017).
[20]A. D. Utyushev, I. L. Isaev, V. S. Gerasimov, A. E. Ershov, V. I. Zakomirnyi, I. L. Rasskazov, S. P. Polyutov, H. Ågren, and S. V. Karpov, "Engineering novel tunable optical high-Q nanoparticle array filters for a wide range of wavelengths," Opt. Express **28**, 1426 (2020).
[21]S. G. Moiseev, I. A. Glukhov, Y. S. Dadoenkova, and F. F. L. Bentivegna, "Polarization-selective defect mode amplification in a photonic crystal with intracavity 2D arrays of metallic nanoparticles," J. Opt. Soc. Am. B **36**, 1645–1652 (2019).
[22]S. Bernadotte, F. Evers, and C. R. Jacob, "Plasmons in molecules," J. Phys. Chem. C **117**, 1863–1878 (2013).
[23]E. Runge and E. K. U. Gross, "Density-functional theory for time-dependent systems," Phys. Rev. Lett. **52**, 997–1000 (1984).
[24]F. Wen, Y. Zhang, S. Gottheim, N. S. King, Y. Zhang, P. Nordlander, and N. J. Halas, "Charge transfer plasmons: Optical frequency conductances and tunable infrared resonances," ACS Nano **9**, 6428–6435 (2015).
[25]V. Kulkarni and A. Manjavacas, "Quantum effects in charge transfer plasmons," ACS Photonics **2**, 987–992 (2015).
[26]T. P. Rossi, A. Zugarramurdi, M. J. Puska, and R. M. Nieminen, "Quantized evolution of the plasmonic response in a stretched nanorod," Phys. Rev. Lett. **115**, 236804 (20150); arXiv:1509.01140.
[27]F. Marchesin, P. Koval, M. Barbry, J. Aizpurua, and D. Sánchez-Portal, "Plasmonic response of metallic nanojunctions driven by single atom motion: Quantum transport revealed in optics," ACS Photonics **3**, 269–277 (2016).
[28]A. Horrer, Y. Zhang, D. Gérard, J. Béal, M. Kociak, J. Plain, and R. Bachelot, "Local optical chirality induced by near-field mode interference in achiral plasmonic metamolecules," Nano Lett. **20**, 509–516 (2020).
[29]R. Esteban, A. G. Borisov, P. Nordlander, and J. Aizpurua, "Bridging quantum and classical plasmonics with a quantum-corrected model," Nat. Commun. **3**, 825 (2012).
[30]R. Esteban, A. Zugarramurdi, P. Zhang, P. Nordlander, F. J. García-Vidal, A. G. Borisov, and J. Aizpurua, "A classical treatment of optical tunneling in plasmonic gaps: Extending the quantum corrected model to practical situations," Faraday Discuss. **178**, 151–183 (2015).
[31]W. Zhu, R. Esteban, A. G. Borisov, J. J. Baumberg, P. Nordlander, H. J. Lezec, J. Aizpurua, and K. B. Crozier, "Quantum mechanical effects in plasmonic structures with subnanometre gaps," Nat. Commun. **7**, 11495 (2016).
[32]S. F. Tan, L. Wu, J. K. W. Yang, P. Bai, M. Bosman, and C. A. Nijhuis, "Quantum plasmon resonances controlled by molecular tunnel junctions," Science **343**, 1496 (2014).
[33]F. Benz, C. Tserkezis, L. O. Herrmann, B. de Nijs, A. Sanders, D. O. Sigle, L. Pukenas, S. D. Evans, J. Aizpurua, and J. J. Baumberg, "Nanooptics of molecular-shunted plasmonic nanojunctions," Nano Lett. **15**, 669–674 (2015).
[34]A. S. Fedorov, P. O. Krasnov, M. A. Visotin, F. N. Tomilin, S. P. Polyutov, and H. Ågren, "Charge-transfer plasmons with narrow conductive molecular bridges: A quantum-classical theory," J. Chem. Phys. **151**, 244125 (2019).
[35]A. S. Fedorov, P. O. Krasnov, M. A. Visotin, F. N. Tomilin, and S. P. Polyutov, "Thermoelectric and plasmonic properties of metal nanoparticles linked by conductive molecular bridges," Phys. Status Solidi B **257**, 2000249 (2020).
[36]R. Landauer, "Electrical resistance of disordered one-dimensional lattices," Philos. Mag. **21**, 863–867 (1970).
[37]W. R. Smythe, *Static and Dynamic Electricity* (Amazon.com, 1950).
[38]V. A. Saranin, "On the interaction of two electrically charged conducting balls," Phys.-Usp. **42**, 385–390 (1999).
[39]Lumerical Solutions, FDTD Solutions, 2020.
[40]L. D. Landau, L. P. Pitaevskii, and E. M. Lifshitz, *Electrodynamics of Continuous Media*, 2nd ed., Course of Theoretical Physics Vol. 2 (Butterworth-Heinemann, 1984).
[41]R. L. Olmon, B. Slovick, T. W. Johnson, D. Shelton, S.-H. Oh, G. D. Boreman, and M. B. Raschke, "Optical dielectric function of gold," Phys. Rev. B **86**, 235147 (2012).

Published under license by AIP Publishing